

Out-of-distribution Detection Using Kernel Density Polytopes

Jayanta Dey,^{1,*} Ashwin De Silva,¹ Will LeVine,¹ Jong Shin,¹ Haoyin Xu,¹ Ali Geisa,¹ Tiffany Chu,¹
Leyla Isik,¹ and Joshua T. Vogelstein¹

Abstract. Any reasonable machine learning (ML) model should not only interpolate efficiently in between the training samples provided (in-distribution region), but also approach the extrapolative or out-of-distribution (OOD) region without being overconfident. Our experiment on human subjects justifies the aforementioned properties for human intelligence as well. Many state-of-the-art algorithms have tried to fix the overconfidence problem of ML models in the OOD region. However, in doing so, they have often impaired the in-distribution performance of the model. Our key insight is that ML models partition the feature space into polytopes and learn constant (random forests) or affine (ReLU networks) functions over those polytopes. This leads to the OOD overconfidence problem for the polytopes which lie in the training data boundary and extend to infinity. To resolve this issue, we propose kernel density methods that fit Gaussian kernel over the polytopes, which are learned using ML models. Specifically, we introduce two variants of kernel density polytopes: *Kernel Density Forest* (KDF) and *Kernel Density Network* (KDN) based on random forests and deep networks, respectively. Studies on various simulation settings show that both KDF and KDN achieve uniform confidence over the classes in the OOD region while maintaining good in-distribution accuracy compared to that of their respective parent models.

1 Introduction For biological agents, experience is not only important to excel in the relevant skills but also to learn where the agent should not be confident at all. From an evolutionary perspective, it is a mandatory property for the biological intelligence to ensure its survival. In short, any intelligent system should get more conscious about its limitations with more experience. However, most of the traditional machine learning models seem to defy this natural law of being intelligent. Although with more training data (experience) they get better at inferring on the samples lying within the convex hull of the training data [1–4], they yield highly confident predictions over the samples lying far away from the training data. Uniform confidence over the classes in the out-of-distribution (OOD) region is crucial for applications like autonomous driving and computer-assisted surgery, where any aberrant reading should be detected and taken care of immediately [1, 5]. An intelligent model capable of detecting OOD data can be a life-saver in these cases.

Intuitively, the easiest solution for OOD sample detection is to learn a function that gives higher scores for in-distribution data and lower scores for OOD data, and thereby re-scale the posterior from the original model accordingly [6]. However, any model that could learn how to detect OOD samples, would have its own problem of being overconfident for the corresponding OOD samples [7, 8]. Again, as mentioned in Hein et al. [1], re-scaling the posteriors cannot solve the OOD overconfidence problem in ReLU (rectified linear unit) networks. Many previous algorithms [1, 7, 9] tried different approaches by modifying the training loss function. Among them, Hein et al. [1] and Hendrycks et al. [7] tried to calibrate the network confidence over the OOD data by exhaustively training the network to be less confident on the OOD data. However, this process would require infinite OOD data for a satisfactory robustness against all possible OOD scenarios. Moreover, these huge OOD data would require a model with larger capacity. At the same time, one can adversarially manipulate an OOD sample to find another OOD sample where the model is overconfident [1, 10, 11]. Erdil et al. [12] proposed kernel density estimation techniques over the features learned at different layers of a deep network and combines the scores

¹ Johns Hopkins University (JHU)

* corresponding author: jdey4@jhu.edu

from all the layers using logistic regression. However, a single model having both good in-distribution performance and OOD robustness is highly desirable.

In this paper, we consider replacing the constant or affine functions learned over the polytopes in random forests and ReLU networks, respectively [1, 4, 13]. We propose two novel kernel density polytope techniques named *Kernel Density Forest* (KDF) and *Kernel Density Network* (KDN). They converge to the true training distribution in the limit when we have infinite training samples for random forests and ReLU networks with sufficient complexity, respectively. At the same time, the estimated likelihood from the kernel density polytopes decreases for samples far away from the training samples. By adding suitable bias to the kernel density estimate, we can achieve uniform posterior over the classes in the OOD region. It completely excludes the need for providing OOD examples to the model. We conduct several simulation studies that show both KDF and KDN are robust against OOD samples while maintain good performance in the in-distribution region.

2 Background In this section, we formulate the problem we are going to address and provide necessary background information about the OOD overconfidence problem in random forests and deep networks.

2.1 Problem Formulation Consider a supervised learning problem with independent and identically distributed training samples $\{(x_i, y_i)\}_{i=1}^N$ such that $(X, Y) \sim \mathcal{P}_{X \times Y}$, where $X \sim \mathcal{P}_{in}$ is a $\mathcal{X} \in \mathbb{R}^d$ valued input and Y is a $\mathcal{Y} = \{1, \dots, K\}$ valued label. We denote the OOD-distribution as \mathcal{P}_{out} with its support spanning the whole feature space excluding the support of \mathcal{P}_{in} . In other words, $\mathcal{P}_{out} := \bigcup_j \mathcal{P}_j$, where \mathcal{P}_j is any distribution having no overlap with \mathcal{P}_{in} . The goal is to learn a model $g : \mathbb{R}^d \times \{\mathbb{R}^d \times \{1, \dots, K\}\}^n \rightarrow [0, 1]^K$ such that,

$$(2.1) \quad g(x) = \begin{cases} P[Y = k|X = x], & \forall k \text{ if } x \sim \mathcal{P}_{in} \\ \frac{1}{K}, & \forall k \text{ if } x \sim \mathcal{P}_{out} \end{cases}$$

where $P[Y = k|X = x]$ is the true posterior probability of class k given by,

$$(2.2) \quad P[Y = k|X = x] = \frac{f_k(x)P[Y = k]}{\sum_{i=1}^K f_i(x)P[Y = i]}$$

Here, $f_i(x)$ is the true class conditional density function of class i . The class prediction \hat{y} for a test sample x is obtained by,

$$(2.3) \quad \hat{y} = \arg \max(g(x))$$

2.2 Overconfidence Problem in Random Forests Random forests (RFs) split the feature space \mathbb{R}^d into a union of axis aligned polytopes Q_r such that $\mathbb{R}^d = \bigcup_{r=1}^p Q_r$, and calculate a constant posterior over those polytopes by counting the number of training samples within each polytope. For instance, the posterior probability of class k w.r.t to the polytope Q_r is given by,

$$(2.4) \quad P[Y = k|x \in Q_r] = \frac{N_{rk}}{N_r}$$

where N_{rk} is the total number of samples with class label y in the polytope Q_r and N_r is the total number of samples in the same polytope. The polytopes lying at the boundary of the training data extend to the whole feature space and hence encompass all the OOD samples. Since the posterior probability for a class is constant across each of those outer polytopes, decision trees and random forests (ensemble of decision trees) tend to be overconfident when making predictions for the OOD inputs.

2.3 Overconfidence Problem in Deep Networks Consider a deep network (DN) $F : \mathbb{R}^d \rightarrow [0, 1]^K$ with $L + 1$ number of layers. If $W^{(l)} \in \mathbb{R}^{u_l \times u_{l-1}}$ is the weight matrix and $b^{(l)} \in \mathbb{R}^{u_l}$ is the bias vector of layer l , then for $x \in \mathbb{R}^d$ we can recursively define the pre- and post-activation output of each layer l ($l = 1, \dots, L + 1$) as,

$$F^{(l)} = W^{(l)}G^{(l-1)}(x) + b^{(l)}$$

and

$$G^{(l)} = \sigma(F^{(l)}(x))$$

respectively. Here, $\sigma(t) = \max\{0, t\}$ is the ReLU activation function and $G^{(0)}(x) = x$.

A trained deep network, at the penultimate layer ($l = L$), induces a finite set of convex polytopes $\{Q_i\}_{i=1}^p$ in the input space \mathbb{R}^d such that $\bigcup_{i=1}^p Q_i = \mathbb{R}^d$. Every point x contained within a polytope Q_i activates the same unique subset of neurons in the network. Therefore, when restricted to Q_i , the penultimate layer output $F^{L+1}(\cdot)$ reduces to an affine function:

$$F^{(L+1)}(x) = V_i^{(L+1)}x + a_i^{(L+1)} \quad \forall x \in Q_i$$

where $V_i^{(L+1)}$ and $a_i^{(L+1)}$ are unique to Q_i . Hein et al. [1] provides explicit expressions for $V_i^{(L+1)}$ and $a_i^{(L+1)}$ in their work.

In summary, a deep network partitions the input space into a finite number of polytopes and learns a unique affine function over each polytope. Since the polytopes located at the training data (in-distribution) boundary extend to infinity, evaluating an affine function over such regions would amount to producing predictions with high confidence scores for inputs that are far away from the training data. This gives rise to the overconfident problem of the deep networks when it comes to OOD inputs.

3 Kernel Density Polytopes In this section, we describe how we fit Gaussian kernels over the polytopes learnt using RFs and DNs, respectively. This leads to the two main contributions of our work, KDFs and KDNs.

3.1 Kernel Density Forests Consider T number of decision trees in a random forest ensemble. Each tree t partitions the feature space into M_t polytopes resulting in a set of $\{\{Q_{t,r}\}_{r=1}^{M_t}\}_{t=1}^T$ polytopes. The intersection of these polytopes gives a new set of polytopes $\{Q_r\}_{r=1}^p$ for the forest. We are interested in fitting a Gaussian kernel $\mathcal{K}_r(\cdot)$ for each polytope Q_r for each class k . Naturally, we would estimate the parameters μ_{rk} and Σ_{rk} of $\mathcal{K}_r(\cdot)$ from the samples with label k contained within Q_r . However, in order to improve the estimates for these parameters, we also incorporate the samples from other polytopes Q_s based on the similarity between Q_r and Q_s .

In order to measure this similarity, for any point $x_r \in Q_r$ with label k , we push every other sample point $x_s \in Q_s$ with the same label down the trees. If the two points end up in the same leaf across all the trees, they belong to the same polytope, i.e. $Q_r = Q_s$. The two points belong to different polytopes ($Q_r \neq Q_s$) if they only share a fraction or none of matching leaves. Hence, we weigh down the contribution from a neighboring polytope Q_s for estimating the kernel in the current polytope Q_r using the following weighting scheme:

$$(3.1) \quad w_{rs} = \begin{cases} \frac{l_{rs}}{T}, & \text{if } Q_r \neq Q_s \\ 1, & \text{if } Q_r = Q_s \end{cases}$$

where l_{rs} is the total number trees x_r and x_s end up in the same leaf node. The higher the weight, the closer two polytopes are to each other in the feature space. With the weights defined above, we

Algorithm 1 Fit a KDX model.

Require:

- (1) M ▷ the parent learner (random forest or deep network model)
- (2) $\mathcal{D}_n = (\mathbf{X}, \mathbf{y}) \in \mathbb{R}^{N \times d} \times \{1, \dots, K\}^N$ ▷ training data

Ensure: g ▷ a KDX model

```
1: function KDX.FIT( $M, \mathbf{X}, \mathbf{y}$ )
2:    $\theta \leftarrow M.FIT(\mathbf{X}, \mathbf{y})$  ▷ train the parent learner
3:   for  $k = 1, \dots, K$  do
4:      $\mathbf{X}_k \leftarrow$  input samples with label  $k$  ▷  $\mathbf{X}_k \in \mathbb{R}^{N_k \times d}$ 
5:      $\{Q_r\}_{r=1}^{m_k} \leftarrow \text{GETPOLYTOPES}(\mathbf{X}_k, \theta)$  ▷  $Q_r = [x_1, \dots, x_{N_{rk}}]$ 
6:     for  $r = 1, \dots, m_k$  do ▷ iterate over each polytope in class  $k$ 
7:        $\mathbf{w}_{rk} \leftarrow \text{COMPUTEWEIGHTS}(Q_r, \mathbf{X}_k, \theta)$  ▷  $\mathbf{w}_{rk} \in [0, 1]^{N_k}$ 
8:        $g.N_{rk} \leftarrow$  number of input samples with weight 1 ▷  $N_{rk}$  is the number of input samples in
           $Q_r$ 
9:        $g.\mu_{rk}, g.\Sigma_{rk} \leftarrow \text{ESTIMATEPARAMETERS}(\mathbf{X}_k, \mathbf{w}_{rk})$  ▷ Estimate parameters using weighted
          MLE
10:    end for
11:  end for
12:  return  $g$ 
13: end function
```

estimate the parameters of kernel $\mathcal{K}_r(\cdot)$ using weighted maximum likelihood estimator over the sample points for each label. By summing over the estimated kernels, we arrive at an estimate $\hat{f}_k(x)$ for the class conditional density:

$$(3.2) \quad \hat{f}_k(x) = \frac{1}{N_k} \sum_{r=1}^p N_{rk} \mathcal{K}_r(x)$$

where N_{rk} is the total number of samples that end up in the current polytope Q_r and $N_k = \sum_{r=1}^p N_{rk}$ is the total number of training samples with class k .

3.2 Kernel Density Networks Consider the deep network F described in section 2.3. We can obtain the set of polytopes $\{Q_{rk}\}_{r=1}^{m_k}$ by grouping the samples having label k that activate the same subset of neurons in the network. Note that $Q_{r_1k} \cap Q_{r_2k} = \emptyset, \forall r_1 \neq r_2$. From Hein et al. [1] it follows that for each $x \in Q_{rk}$, the pre-activation function $F^{(l)}(x)$ of layer l reduces to the affine function $V_{rk}^{(l)}x + a_{rk}^{(l)}$, for $l = 1, \dots, L$.

We are interested in fitting a Gaussian kernel $\mathcal{K}_r(\cdot)$ over the polytope Q_{rk} . The simplest way of estimating the mean μ_{rk} and bandwidth (covariance) matrix Σ_{rk} of $\mathcal{K}_r(\cdot)$ is to estimate them from the $|Q_{rk}| = N_{rk}$ number of training samples within Q_{rk} . However, in order to improve the kernel parameter estimates we also incorporate samples that lie within a neighborhood of Q_{rk} . To this end, we employ a weighting function $w(\cdot)$ that assigns a weight of 1 for samples within Q_{rk} and decreasing weights for input samples outside Q_{rk} as they move away from it:

$$(3.3) \quad w(x) = \begin{cases} \exp(-d/h), & \text{if } \exp(-d/h) \geq T \\ 0, & \text{else} \end{cases}$$

Algorithm 2 Computing weights in KDF

Require:

- (1) Q_r ▷ a polytope in class k
- (2) $\mathbf{X}_k \in \mathbb{R}^{N_k \times d}$ ▷ input samples with class label k
- (3) θ ▷ parent random forest model

Ensure: $\mathbf{w} \in [0, 1]^{N_k}$ ▷ weights for each input sample in class k

- 1: **function** COMPUTEWEIGHTS($Q_r, \mathbf{X}_k, \theta$)
 - 2: $\mathbf{L} \leftarrow \text{PUSHDOWNTREES}(\mathbf{X}_k)$ ▷ push the samples \mathbf{X}_k down the T trees in total and store the leaf number they end up in $\mathbf{L} \in \mathbb{R}^{N \times T}$
 - 3: $\mathbf{l} \leftarrow \text{COUNTMATCHES}(\mathbf{L})$ ▷ count the number times the samples end up in the leaf as those for the samples in the current polytope and $\mathbf{l} \in \mathbb{R}^{N_k}$
 - 4: $\mathbf{w} \leftarrow \frac{1}{T}$
 - 5: **return** \mathbf{w}
 - 6: **end function**
-

where

$$(3.4) \quad d = \sum_{l=1}^L \|F^{(l)}(x) - (V_{rk}^{(l)}x + a_{rk}^{(l)})\|_2$$

For a given sample x , (3.4) measures the difference between pre-activation output of each layer and the affine restriction of Q_{rk} at that layer across the network. It is apparent that $d = 0$ for every $x \in Q_{rk}$ and d gets higher as x moves away from Q_{rk} . This measure is converted to a weight within $[0, 1]$ by (3.3). T is a threshold used to set the extremely small weights to zero, and h is a parameter that controls the neighborhood size.

Based on the weights above, we estimate the parameters of $\mathcal{K}_r(\cdot)$ from the samples having label k using the weighted maximum likelihood estimator.

By summing over the kernels learnt over each Q_{rk} , we arrive at the class conditional density estimate $\hat{f}_k(x)$:

$$(3.5) \quad \hat{f}_k(x) = \frac{1}{N_k} \sum_{r=1}^{m_k} N_{rk} \mathcal{K}_r(x)$$

where, $N_k = \sum_{r=1}^{m_k} N_{rk}$ is the total number of training samples in class k .

3.3 Inference So far we have the class conditional densities estimated in (3.2) and (3.5). Note that these density functions are estimated as summation of Gaussian kernels. Hence, the likelihoods out of these functions decrease for sample points far away from the training samples. We can exploit this phenomenon to detect OOD samples. To be specific, we add the a bias to the class conditional density \hat{f}_k :

$$(3.6) \quad \tilde{f}_k(x) = \hat{f}_k(x) + \delta$$

where the bias is given by

$$(3.7) \quad \delta = \frac{\min(\{\min(\{\hat{f}_k(x_i)\}_{i=1}^{N_k})\}_{k=1}^K)}{CN}$$

Algorithm 3 Computing weights in KDN

Require:

- (1) Q_r ▷ a polytope in class k
- (2) $\mathbf{X}_k \in \mathbb{R}^{N_k \times d}$ ▷ input samples with class label k
- (3) θ ▷ parent deep network model with parameters $\{\mathbf{W}_l, \mathbf{b}_l\}_{l=1}^{L+1}$

Ensure: $\mathbf{w} \in [0, 1]^{N_k}$ ▷ weights for each input sample in class k

```
1: function COMPUTEWEIGHTS( $Q_r, \mathbf{X}_k, \theta$ )
2:    $\{\mathbf{W}_l, \mathbf{b}_l\}_{l=1}^{L+1} \leftarrow \theta$ 
3:    $\mathbf{A}_0 \leftarrow \mathbf{X}_k^\top$ 
4:    $\mathbf{A}_{0,ref} \leftarrow \mathbf{X}_k^\top$ 
5:    $\mathbf{d} = 0$  ▷  $\mathbf{d} \in \mathbb{R}^{n_k}$ 
6:   for  $l = 1, \dots, L$  do
7:      $\mathbf{m}_l \leftarrow$  ReLU activation pattern induced by any  $x \in Q_r$  in the layer  $l$  of  $\theta$ 
8:      $\mathbf{Z}_l \leftarrow \mathbf{W}_l \mathbf{A}_{l-1} + \mathbf{b}_l$ 
9:      $\mathbf{A}_l \leftarrow \text{ReLU}(\mathbf{Z}_l)$ 
10:     $\mathbf{Z}_{l,ref} \leftarrow \mathbf{W}_l \mathbf{A}_{l-1,ref} + \mathbf{b}_l$ 
11:     $\mathbf{A}_{l,ref} \leftarrow \text{diag}(\mathbf{m}_l) \mathbf{Z}_{l,ref}$ 
12:     $\mathbf{d} \leftarrow \mathbf{d} + d(\mathbf{A}_l - \mathbf{A}_{l,ref})$  ▷  $d(\mathbf{M}_{r \times c}) \in \mathbb{R}^c$  returns the L2-norms of the column vectors of  $\mathbf{M}$ 
13:  end for
14:   $\mathbf{w} \leftarrow e^{-\mathbf{d}/h}$ 
15:   $\mathbf{w} \leftarrow \text{THRESHOLD}(\mathbf{w}, T)$  ▷ Set the weights less than  $T$  to zero
16:  return  $\mathbf{w}$ 
17: end function
```

where C is a constant. Intuitively, the point in the training sample which yields minimum likelihood out of \hat{f}_k lies in the training data boundary. By multiplying it with a suitable constant, we can make \hat{f}_k in (3.6) dominant compared to the bias in the in-distribution region whereas the bias term would dominate in the OOD region. Note that in 3.7, $\delta \rightarrow 0$ as the total training points, $N \rightarrow \infty$. Now the inference step is common to both KDF and KDN. During inference, the class posterior probability (confidence) $\hat{P}[Y = k|X = x]$ of class k for a test point x is estimated using the Bayes rule as follows:

$$(3.8) \quad \hat{P}[Y = k|X = x] = \frac{\tilde{f}_k(x) \hat{P}[Y = k]}{\sum_{i=1}^K \tilde{f}_i(x) \hat{P}[Y = i]}$$

where $\hat{P}[Y = k]$ is the prior probability of class k estimated from the training data.

4 Experiments In this section, we illustrate how KDFs and KDNs perform better than their respective parent models on simulation datasets. We also demonstrate how our algorithms' posterior estimates better correspond to those of human intelligence.

4.1 Simulations We construct five types of binary class simulations:

- *Gaussian XOR* is a two-class classification problem with equal class priors. Conditioned on being in class 0, a sample is drawn from a mixture of two Gaussians with means $\pm[0.5, -0.5]^\top$ and standard deviations of 0.25. Conditioned on being in class 1, a sample is drawn from a mixture of two Gaussians with means $\pm[0.5, -0.5]^\top$ and standard deviations of 0.25.
- *Spiral* is a two-class classification problem with the following data distributions: let K be the

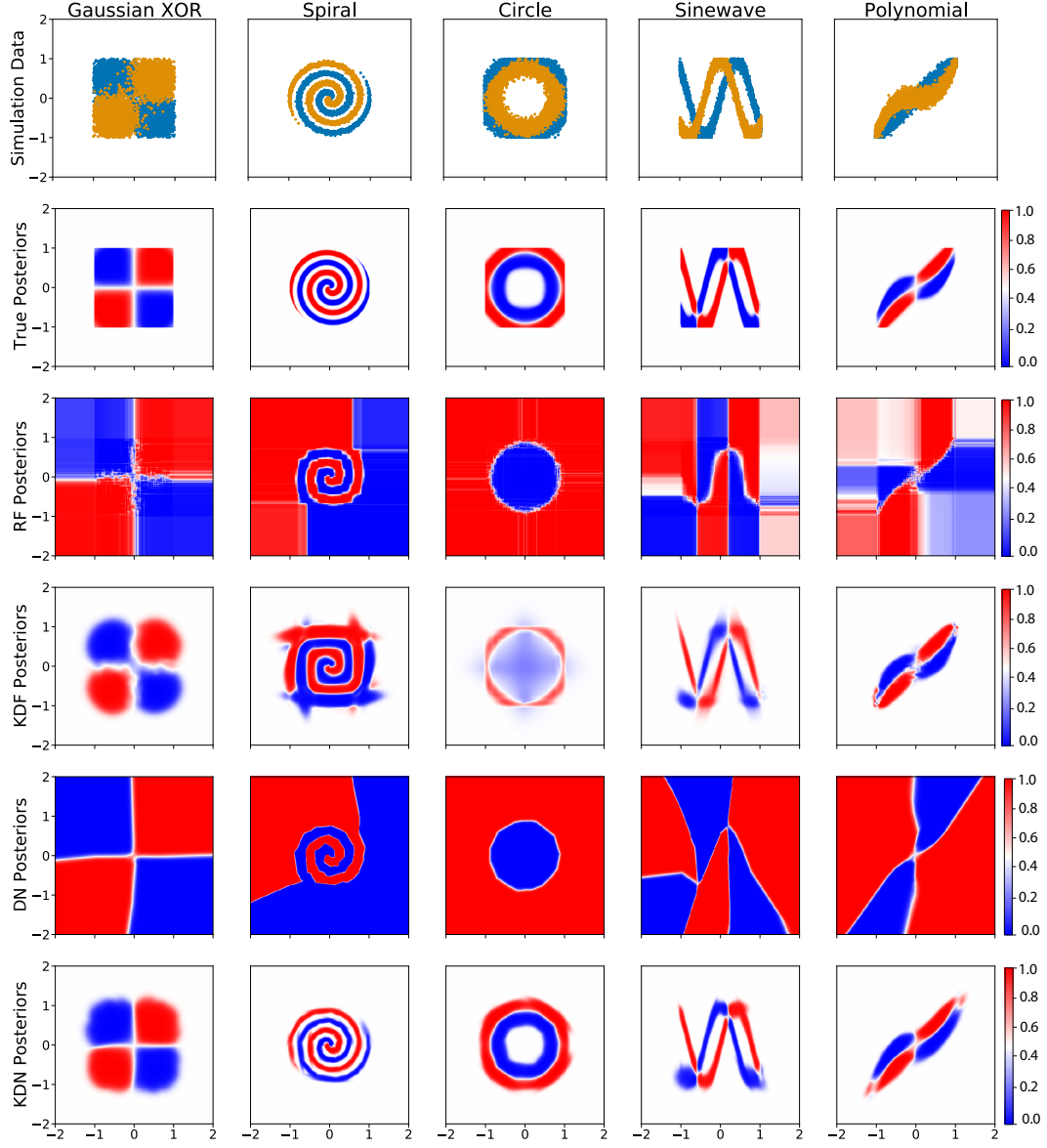


Figure 1: Simulation distributions and posterior estimates by different algorithms. Binary simulation data are generated within the region bounded by $[-1, 1] \times [-1, 1]$, then posteriors are estimated within the $[-2, 2] \times [-2, 2]$ region. Kernel Density Forests (KDFs) and Kernel Density Networks (KDNs) yield better estimates when compared to their respective parent models—random forests (RFs) and ReLU deep networks (DNs). They achieve particularly good posteriors in the out-of-distribution (OOD) region, while RFs and DNs yield overconfident posteriors.

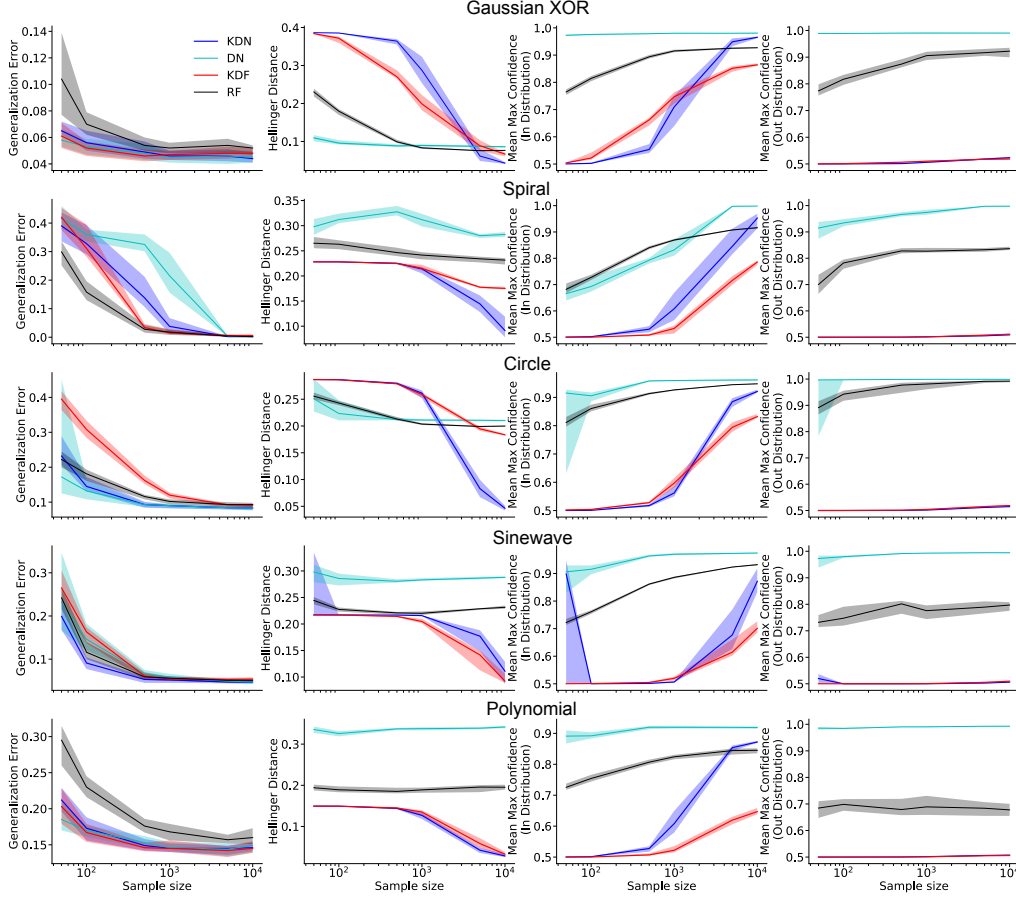


Figure 2: Binary classifications on simulation data. Each line shows median results from 45 repetitions and the shadowed regions represent the 25 and 75-th quantiles.

number of classes and $S \sim \text{multinomial}(\frac{1}{K} \vec{1}_K, n)$. Conditioned on S , each feature vector is parameterized by two variables, the radius r and an angle θ . For each sample, r is sampled uniformly in $[0, 1]$. Conditioned on a particular class, the angles are evenly spaced between $\frac{4\pi(k-1)t_K}{K}$ and $\frac{4\pi(k)t_K}{K}$, where t_K controls the number of turns in the spiral. To inject noise along the spirals, we add Gaussian noises to the evenly spaced angles $\theta' : \theta = \theta' + \mathcal{N}(0, 0.09)$. The observed feature vector is then $(r \cos(\theta), r \sin(\theta))$.

- *Circle* is a two-class classification problem with equal class priors. Conditioned on being in class 0, a sample is drawn from a circle centered at $(0, 0)$ with a radius of $r = 0.75$. Conditioned on being in class 1, a sample is drawn from a circle centered at $(0, 0)$ with a radius of $r = 1$, which is cut off by the region bounds. To inject noise along the circles, we add Gaussian noises to the circle radii $r' : r = r' + \mathcal{N}(0, 0.01)$.

	RF		KDF		DN		KDN	
Simulation	AUROC	FPR@95	AUROC	FPR@95	AUROC	FPR@95	AUROC	FPR@95
Gaussian XOR	0.80(± 0.03)	0.83(± 0.13)	0.98(± 0.00)	0.32(± 0.28)	0.14(± 0.01)	0.93(± 0.05)	0.98(± 0.01)	0.41(± 0.37)
Spiral	0.55(± 0.02)	0.75(± 0.16)	0.99(± 0.00)	0.39(± 0.36)	0.33(± 0.10)	0.97(± 0.04)	0.99(± 0.00)	0.39(± 0.38)
Circle	0.29(± 0.13)	0.81(± 0.19)	0.97(± 0.00)	0.32(± 0.25)	0.02(± 0.00)	0.87(± 0.14)	0.99(± 0.00)	0.34(± 0.31)
Sinewave	0.86(± 0.03)	0.68(± 0.11)	0.99(± 0.00)	0.31(± 0.27)	0.29(± 0.01)	0.88(± 0.12)	0.99(± 0.00)	0.31(± 0.29)
Polynomial	0.82(± 0.03)	0.64(± 0.14)	0.99(± 0.00)	0.28(± 0.26)	0.08(± 0.01)	0.79(± 0.20)	0.99(± 0.00)	0.28(± 0.26)

Table 1: Performance metrics on the out-of-distribution (OOD) region: area under the receiver operating characteristic (AUROC) and false negative rates at 95% recall (FPR@95).

- *Sinewave* is a two-class classification problem based on sine waves. Conditioned on being in class 0, a sample is drawn from the distribution $y = \cos(\pi x)$. Conditioned on being in class 1, a sample is drawn from the distribution $y = \sin(\pi x)$. We inject Gaussian noises to the sine wave heights $y' : y = y' + \mathcal{N}(0, 0.01)$.
- *Polynomial* is a two-class classification problem with the following data distributions: $y = x^a$. Conditioned on being in class 0, a sample is drawn from the distribution $y = x^1$. Conditioned on being in class 1, a sample is drawn from the distribution $y = x^3$. Gaussian noises are added to variables $y' : y = y' + \mathcal{N}(0, 0.01)$.

As in Figure 1, all data samples (10,000 per simulation) are bounded within the $[-1, 1] \times [-1, 1]$ region and equally divided into two classes (5,000 per class). We evaluate model performance of RFs, KDFs, DNs, and KDNs using in-distribution generalization errors, in-distribution Hellinger distances between true and estimate class posteriors, area under the receiver operating characteristic (AUROC), false positive rate at 95 recall (FPR@95), and mean maximum confidence scores for both in-distribution and OOD regions [1]. We consider the the annular region between $[-1, 1] \times [-1, 1]$ and $[-5, 5] \times [-5, 5]$ as the OOD region for the purpose of computing the relevant evaluation metrics.

4.2 Machine Experiments Five types of simulation data (Section 4.1) are sampled within $[-1, 1] \times [-1, 1]$ to fit KDFs and KDNs along with their respective parent models: RFs and DNs. Each parent random forest has 500 trees, and each tree is split until class purity. Each parent deep network has four hidden layers with 10 nodes in each layer and is trained using the Adam optimizer at a learning rate of 3×10^{-4} . Figure 1 illustrates the posteriors learned using these four models along with the true posteriors. It is apparent that RFs and DNs yield highly confident predictions outside the in-distribution regions, demonstrating their overconfidence problems. Meanwhile, both KDFs and KDNs yield uniform posteriors (0.5) over the classes outside $[-1, 1] \times [-1, 1]$, which is consistent with human intelligence as described in Section 4.3. Furthermore, KDFs and KDNs also improve the posteriors within the in-distribution regions, showing no compromise while overcoming the overconfident problems in their parent models.

Figure 2 reports the algorithms’ in-distribution performance and confidence scores in both in-distribution and OOD regions. In terms of generalization error, both KDFs and KDNs achieve similar or even better performance compared to that of their respective parent models. Furthermore, our proposed models always achieve posteriors closer to the true posteriors compared to those of RFs and DNs, as illustrated in the Hellinger distance curves (Figure 2, second column). The mean maximum confidence scores for both KDFs and KDNs become comparable with those of their parent models only at large sample sizes for the in-distribution region (Figure 2, third column), which are more reasonable. More interestingly, for KDFs and KDNs, the mean maximum confidence scores in the OOD regions always stay around 0.5. In stark contrast to that, RFs and DNs maintain very high scores (close to 1) in the OOD regions, which correspond to their overconfident posteriors (Figure 1).

Again, in Table 1, we show the OOD performance of KDFs and KDNs along with their parent models. RFs perform better than DNs in detecting OOD inputs, which is also evident in the human experiments (Section 4.3). However, both KDFs and KDNs are significantly better than RFs and DNs in terms of AUROC and FPR@95 for OOD detection. The two overconfident parent models result in a much higher number of false positives.

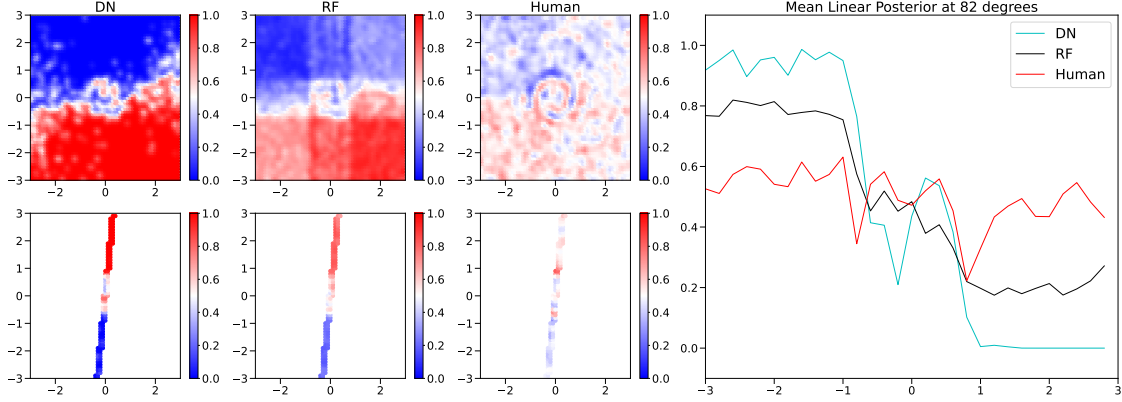


Figure 3: Linear evaluation of posterior estimates by reference algorithms and 126 human subjects. Binary spiral simulation data are generated within the region bounded by $[-1, 1] \times [-1, 1]$, then posteriors are estimated within the $[-3, 3] \times [-3, 3]$ region. The line plot (**right**) shows the mean posteriors over affine lines at 82 degrees (**left bottom**). In the out-of-distribution region, Humans generate reasonable mean posteriors around chance probabilities (0.5), while ReLU deep networks with a single hidden layer (DNs) and random forests (RFs) become much more confident.

4.3 Human Experiments To assess our assumptions about OOD confidence of natural intelligence, we also conducted experiments with human subjects. Two types of simulations are used for the experiments: Gaussian XOR and Spiral (Section 4.1). We recruited 150 participants from the Amazon Mechanical Turks platform. The participants were provided with basic instructions and the structural information regarding the experiments. They were subsequently asked to start the experiments where each individual was exposed to 100 trials of randomly chosen Gaussian XOR and Spiral simulations. Each simulation visualizes 100 randomly distributed points parameterized to aforementioned simulations confined within the $[-1, 1] \times [-1, 1]$ region. The participants were asked to provide a single estimate of confidence per each trial for a randomly distributed test point over the range of $[-3, 3] \times [-3, 3]$. Of 150 participants, 24 subjects were excluded from the analyses for failing to meet the following two criteria: 1. pass at least 4 out of 5 catch trials designed to challenge attention 2. do not miss more than 1% of the data.

We analyzed the enumerated posterior estimates at all test points and their corresponding 2-dimensional coordinates. Figure 3 shows the estimated posteriors along a line at 82° through the origin at $(0, 0)$. We can see human subjects give uniform posterior over the classes, i.e. 0.5 as we move farther away from the data convex hull specified by $[-1, 1] \times [-1, 1]$. In contrast, random forest and deep net models show significantly more confident posteriors in OOD regions than in-distribution regions. The results further confirm that, in terms of OOD detection, our algorithms built on kernel density polytopes resemble natural intelligence, avoiding the overconfidence of RFs and DNs.

5 Discussion In this paper, we have introduced a simple concept—replace the constant or affine function in each polytope of an ML model with a Gaussian kernel, which is locally fitted over the data within the corresponding and the neighboring polytopes. This leads to a lower class conditional like-

likelihood for sample points far away from the convex hull of the training data compared to that for the sample points within in-distribution region. Adding a suitable bias to all the class conditional likelihoods makes this bias dominate in the OOD region yet negligible in the in-distribution region. Such a method results in the uniform posteriors over the classes in the OOD region without using OOD data for training. Experiments with human subjects show that this property corresponds with human intelligence. Thus, KDFs and KDNs could be used to further explore how natural intelligence evaluates OOD information with existing knowledge.

Our proposed methods can have useful applications in learning scenarios like lifelong [14] and OOD learning [15], where the detection of OOD data can enable better transfer of knowledge between tasks. Moreover, the kernel density polytopes could be extended to many other algorithms, including convolutional neural networks. In other words, we can take the output from a certain layer in convolutional networks and fit a kernel density convolutional neural network (KDCNN) model that can achieve similar properties on image data. This could motivate future works on a KDCNN model that is robust to OOD data and adversarial attacks.

In conclusion, kernel density polytopes enable OOD detection without sacrificing any in-distribution performance. Models augmented with such a method could achieve better overall performance than the original and produce posteriors that resemble human decisions. In the meantime, our code, including the package and the experiments in this manuscript, is available from <https://github.com/neurodata/kdg>.

Acknowledgements The authors thank the support of the NSF-Simons Research Collaborations on the Mathematical and Scientific Foundations of Deep Learning (NSSF grant 2031985). This work is graciously supported by the Defense Advanced Research Projects Agency (DARPA) Lifelong Learning Machines program through contracts FA8650-18-2-7834 and HR0011-18-2-0025. Research was partially supported by funding from Microsoft Research and the Kavli Neuroscience Discovery Institute.

References

- [1] Matthias Hein, Maksym Andriushchenko, and Julian Bitterwolf. Why relu networks yield high-confidence predictions far away from the training data and how to mitigate the problem. In *Proceedings of the IEEE/CVF Conference on Computer Vision and Pattern Recognition*, pages 41–50, 2019.
- [2] Chuan Guo, Geoff Pleiss, Yu Sun, and Kilian Q. Weinberger. On calibration of modern neural networks. In Doina Precup and Yee Whye Teh, editors, *Proceedings of the 34th International Conference on Machine Learning*, volume 70 of *Proceedings of Machine Learning Research*, pages 1321–1330. PMLR, 06–11 Aug 2017.
- [3] Agustinus Kristiadi, Matthias Hein, and Philipp Hennig. Being bayesian, even just a bit, fixes overconfidence in ReLU networks. In Hal Daumé III and Aarti Singh, editors, *Proceedings of the 37th International Conference on Machine Learning*, volume 119 of *Proceedings of Machine Learning Research*, pages 5436–5446. PMLR, 13–18 Jul 2020.
- [4] Haoyin Xu, Kaleab A. Kinfu, Will LeVine, Sambit Panda, Jayanta Dey, Michael Ainsworth, Yu-Chung Peng, Madi Kusmanov, Florian Engert, Christopher M. White, Joshua T. Vogelstein, and Carey E. Priebe. When are Deep Networks really better than Decision Forests at small sample sizes, and how? *arXiv preprint arXiv:2108.13637*, 2021.
- [5] Alexander Meinke, Julian Bitterwolf, and Matthias Hein. Provably robust detection of out-of-distribution data (almost) for free. *arXiv preprint arXiv:2106.04260*, 2021.

- [6] Shiyu Liang, Yixuan Li, and Rayadurgam Srikant. Enhancing the reliability of out-of-distribution image detection in neural networks. arXiv preprint arXiv:1706.02690, 2017.
- [7] Dan Hendrycks, Mantas Mazeika, and Thomas Dietterich. Deep anomaly detection with outlier exposure. arXiv preprint arXiv:1812.04606, 2018.
- [8] Eric Nalisnick, Akihiro Matsukawa, Yee Whye Teh, Dilan Gorur, and Balaji Lakshminarayanan. Do deep generative models know what they don't know? arXiv preprint arXiv:1810.09136, 2018.
- [9] Terrance DeVries and Graham W Taylor. Learning confidence for out-of-distribution detection in neural networks. arXiv preprint arXiv:1802.04865, 2018.
- [10] Anh Nguyen, Jason Yosinski, and Jeff Clune. Deep neural networks are easily fooled: High confidence predictions for unrecognizable images. In Proceedings of the IEEE conference on computer vision and pattern recognition, pages 427–436, 2015.
- [11] Vikash Sehwal, Arjun Nitin Bhagoji, Liwei Song, Chawin Sitawarin, Daniel Cullina, Mung Chiang, and Prateek Mittal. Better the devil you know: An analysis of evasion attacks using out-of-distribution adversarial examples. arXiv preprint arXiv:1905.01726, 2019.
- [12] Ertunc Erdil, Krishna Chaitanya, and Ender Konukoglu. Unsupervised out-of-distribution detection using kernel density estimation. arXiv preprint arXiv:2006.10712, 2020.
- [13] Leo Breiman. Random Forests. Machine Learning, 45(1):5–32, 2001.
- [14] Jayanta Dey, Joshua Vogelstein, Hayden Helm, Will Levine, Ronak Mehta, Ali Geisa, Haoyin Xu, Gido van de Ven, Emily Chang, Chenyu Gao, et al. Representation ensembling for synergistic lifelong learning with quasilinear complexity. 2022.
- [15] Ali Geisa, Ronak Mehta, Hayden S. Helm, Jayanta Dey, Eric Eaton, Carey E. Priebe, and Joshua T. Vogelstein. Towards a theory of out-of-distribution learning. _eprint: 2109.14501, 2021.